Regulation of virion production by the ORF8 signal peptide across SARS-CoV-2 variants

Mir M. Khalid[1,2], Irene P. Chen[1,2], Frank S. Soveg[1,2], Taha Y. Taha[1,2],Takako Tabata[1,2], Rahul K. Suryawanshi[1,2], Abdullah M. Syed[1,5], Alison Ciling[1,5], Maria McCavitt-Malvido[1,2], Ursula Schulze-Gahmen[1,2], Jennifer Hayashi[1,2], Ik-Jung Kim[3], Siew Wai Fong[6], Jyoti Batra[2,10-12], G. Renuka Kumar[1,2], Laurent Renia[6,7], Lisa FP Ng[6], Nevan J. Krogan[2,10-12], Jennifer A. Doudna[1,4,5], Eric Verdin[3], Melanie Ott[1,2,8,9*].

[1]Gladstone Institute of Virology, Gladstone Institutes, San Francisco, CA, USA.

[2]University of California, San Francisco (UCSF), San Francisco, CA, USA.

[3] Buck Institute for Research on Aging, Novato, CA, USA.

[4]HHMI, University of California, Berkeley, CA, USA.

[5]Innovative Genomics Institute, University of California, Berkeley, CA, USA.

[6]A*STAR Infectious Diseases Labs (A*STAR ID Labs), Agency for Science, Technology and Research (A*STAR), Singapore, Singapore.

[7]Lee Kong Chian School of Medicine, Nanyang Technological University, Singapore, Singapore.

[8]Quantitative Biosciences Institute COVID-19 Research Group (QCRG), University of California San Francisco, San Francisco, CA, USA

[9]Chan Zuckerberg Biohub, San Francisco, CA, USA

20 [10]Quantitative Biosciences Institute (QBI), University of California, San Francisco; San
21 Francisco, CA 94158, USA.
22
23
24 [11]Department of Cellular and Molecular Pharmacology, University of California, San
25 Francisco, San Francisco, CA 94158, USA.
26
27 [12]Gladstone Institute of Data Science and Biotechnology, J. David Gladstone Institutes;
28 San Francisco, CA 94158, USA.
29
30
31 Mir M. Khalid, Irene P. Chen, Frank S. Soveg contributed equally to this article.
32 The authors declare no conflict of interest.
33 * For correspondence: Melanie Ott, melanie.ott@gladstone.ucsf.edu
34

Abstract

The open reading frame 8 (ORF8), an accessory protein of SARS-CoV-2, is prone to deletions and mutations across different viral variants, which was first described in several Singapore variants. The reason why viral evolution favors loss or inactivation of ORF8 is not fully understood, although the effects of ORF8 on inflammation, immune evasion, and disease severity have been described. Here we show –using clinical ORF8-deficient viral isolates, virus-like particles (VLPs) and viral replicons– that ORF8 expression dampens viral particle production. ORF8 physically interacts with the viral Spike protein and induces Golgi fragmentation, overall contributing to less virus particle production. Using systematic ORF8 deletions, we mapped the particle-reducing function to its N-terminal signal peptide. Interestingly, this part of ORF8 is severely truncated in the recent XBB.1.5 variant, and when restored, suppresses viral particle production in the context of the entire viral genome. Collectively, our data support the model that evolutionary pressure exists to delete ORF8 sequence and expression across SARS-CoV-2 variants to fully enable viral particle production.

Keywords: SARS-CoV-2, ORF8, Spike, VLP, replication, XBB.1.5, Signal peptide.

56 **Importance**

57 SARS-CoV-2 variants continue to emerge worldwide with advantages in
58 replication and immune evasion. Many variants have acquired distinct mutations in
59 independent lineages to abolish ORF8 expression. To understand the molecular
60 mechanisms behind this evolutionary trend, we utilized reverse genetics, molecular
61 virology, and confocal microscopy to show that ORF8 has antiviral functions by
62 dampening viral particle production and inducing Golgi stress during infection. Our data
63 demonstrate that SARS-CoV-2 is continuing its adaption to optimize viral particle
64 production and other unknown aspects of viral infection.

65

66

67

68

69

70

71

72

73

74

75 **Introduction**

76 Since the beginning of the COVID-19 pandemic, numerous SARS-CoV-2
77 variants have and continue evolving with enhanced spread and antibody neutralization
78 escape. . The SARS-CoV-2 Spike protein has evolved the most with mutations altering
79 its entry and immune evasion functions . Open reading frame 8 (ORF8) is a SARS-CoV-
80 2 accessory protein that has also undergone continuous evolution since the beginning
81 of the pandemic (**Fig S1**) and is often truncated in emerging viral variants without an
82 apparent decrease in viral fitness (1–4). One such viral variant is an isolate from
83 Singapore, where a 382- nucleotide deletion removed almost the entire ORF8 sequence
84 as well as the 3'-end of ORF7b (5). Many other ORF8 mutations are common in
85 circulating SARS-CoV-2 variants. Mutation S84L is now considered a lineage-defining
86 mutation that is fixed in all circulating SARS-CoV-2, including all major variants of
87 concerns (VOCs) and variants of interest (VOIs) (6) (**Fig S1**). The Alpha variant
88 featured Q27Stop leading to the expression of a t runcated protein (4,7). Similarly, a
89 recent Omicron subvariant XBB.1.5 has an even shorter truncated ORF8 due to G8Stop
90 mutation, which has been observed in all XBB.1.5-descendent variants including
91 XBB.1.16, XBB.1.16, EG.1, EG.5 (4). Despite the many ways ORF8 expression is
92 eliminated in SARS-CoV-2 variants, there was no apparent decrease in viral fitness as
93 some of the variants have dominated globally. Hence, intact ORF8 might be deleterious
94 to certain aspects of the viral life cycle

95

96 Many studies have demonstrated that ORF8 is involved in immune modulation
97 thereby likely being pro-viral. For example, ORF8 downregulates MHC-I expression and
98 interferon responses (8,9). A characteristic feature of ORF8 is that it is secreted from
99 infected cells and is readily detected in COVID-19 patient sera (1,10). As such, the
100 protein has pro-inflammatory properties and binds for example to the IL17 receptor A
101 (IL17RA), which might harm the host and thus suppress viral replication in the long-term
102 (5,11–15). Overall, the role of ORF8 during viral replication is pleiotropic and not yet
103 fully understood.

104 In the cell, ORF8 is an ER luminal protein, which binds and colocalizes with the
105 Spike protein when co-expressed (16,17). ORF8 must transit through the Golgi for
106 proper modification and secretion with the viral structural proteins that are also
107 secreted. Structural proteins during this transit assemble into a viral particle and leave
108 the cell as virions, while ORF8 has been shown to form dimers, adopting an
109 immunoglobulin-like structure with an N-terminal 15-amino acid signal peptide that
110 allows entry into the ER lumen (16,18,19). Once secreted, ORF8 elicits proinflammatory
111 reactions through multiple host protein interactions, including binding to the IL-17RA
112 (12,14,20). Here, we propose that its transit through the secretory pathway in the
113 presence of the viral structural proteins, specifically Spike, allows ORF8 to regulate viral
114 particle production directly. We test this hypothesis with virus-like particles (VLPs) that
115 resemble authentic viral particles containing all four viral structural proteins packaging
116 cargo genomes containing a SARS-CoV-2 packaging signal (21). Using this tool and
117 reverse genetics, we investigated the impact of ORF8 on virion production.

118

119 **Results**

120 **ORF8 expression reduces virion production but not genome replication**

121 First, we compared the infectious virion production of the ancestral isolate WA1,
122 which does not contain mutations in ORF8, and of the Singapore Isolate (abbreviated
123 Sing), which lacks most of the ORF8 sequence (del27849_28230 (ORF8Δaa1-112)).
124 We found that the Singapore isolate produces markedly more infectious virions than the
125 WA1 isolate, supporting a model where ORF8 negatively regulates the viral life cycle
126 (**Fig.1A**). To determine whether viral RNA replication is specifically involved, we turned
127 to a replicon system based on the WA1 genome in which we replaced the Spike coding
128 region with a secreted nano-luciferase (nLuc) reporter and eGFP (22). The lack of Spike
129 prevents production of infectious virus upon infection. We generated a replicon lacking
130 ORF8 expression by inserting a stop codon at the second amino acid (Rep-ORF8-Stop)
131 (**Fig. 1B**). We transfected BHK-21 cells with either replicon plasmids along with a
132 nucleocapsid protein (N) expression vector necessary to launch viral replication (22–25)
133 (22–25) (**Fig.1B and Fig. S2B**). As part of viral replication, the Spike sgRNA will instead
134 produce nLuc that is secreted into the supernatant. Therefore, luminescence from the
135 cell culture media serves as a proxy for viral RNA replication as has been validated
136 previously (22). We did not observe any difference in luminescence between the WA1
137 and the Rep-ORF8-Stop replicons (**Fig.1B**), indicating that ORF8 expression does not
138 affect RNA replication.

139

140 Next, we repeated the assay but included a Spike expression vector in the
141 transfection to produce single-round infectious viral particles. These particles can be
142 used to perform single round infection in Vero ACE2 and TMPRSS2 cells.
143 Luminescence signal after infection indicate the infectious titer of the generated single-
144 round infectious particles. To investigate the effect of ORF8 expression on particle
145 production, we used the Rep-ORF8-Stop construct and co-expressed Strep-tagged
146 ORF8 -or eGFP control plasmid along with the Spike and N expression vectors (**Fig.**
147 **1C**). We found that ORF8 expression in producer cells significantly reduced the
148 production of single-round infectious particles (**Fig. 1D**). We conclude that ORF8 has a
149 negative impact on particle production or entry but does not affect viral RNA replication.

150 **ORF8 colocalizes with Spike in Cis-Golgi and causes Golgi stress response in**
151 **infected cells**

152 During infection, SARS-CoV-2 structural proteins S, N, M, and E as well as
153 genomic RNA assemble at the ER-Golgi intermediate compartment (ERGIC) to produce
154 infectious virions. We previously showed that ORF8 is an ER-luminal protein and
155 interacts with Spike when overexpressed (16). To determine whether virally produced
156 ORF8 colocalizes with Spike during infection, we infected A549-ACE2 cells with the
157 WA1 and Singapore clinical isolates, and examined ORF8 and Spike localization
158 relative to GM130, a cis-Golgi marker. ORF8 and Spike colocalized with GM130 only in
159 WA1-infected cells (**Fig. 2 and Fig. S3**). In addition, we observed Golgi fragmentation
160 and dispersion in WA1-infected cells, whereas in mock- and Singapore-infected cells,
161 the GM130 signal showed a normal dotted pattern near the nucleus, despite high viral
162 particle production in the latter case. This indicates that ORF8 compromises the

163 integrity of the cellular Golgi apparatus similarly to what was previously observed upon
164 SARS-CoV-2, flavivirus infection, and flavivirus NS1 protein expression (26–28). These
165 data indicate that ORF8 colocalizes with Spike in intracellular ER-Golgi compartments
166 during infection, which appear disrupted and fragmented over time only when ORF8 is
167 present.

168 **ORF8 reduces VLP production but not VLP entry**

169 To further define the effect of ORF8 on virion production, we generated VLPs in
170 the presence or absence of ORF8. Similar to replicon particles, VLPs are an authentic
171 tool for investigating SARS-CoV-2 viral particle production and entry (21,29) as they
172 also contain the four viral structural proteins S, N, M, and E but instead of a modified or
173 intact viral genome, they package a reporter RNA with containing the packaging
174 sequence, named T20 (21). To this end, we transfected HEK-293T cells (producer cells)
175 with plasmids expressing SARS-CoV-2 S, N, M, and E proteins, a reporter plasmid
176 containing the T20 packaging signal and firefly luciferase and a plasmid expressing
177 either eGFP or ORF8 (**Fig. 3A**). Once expressed in HEK-293T cells, the structural
178 proteins assemble VLPs that contain the T20 reporter RNA and are released into the
179 culture medium. These VLPs are then used to infect HEK293T-ACE2-TMPRSS2
180 (receiver cells). The luminescence from infected cells is a measurement of the VLP titer
181 (21). In a dose-dependent manner, we confirmed that VLPs produced in the presence of
182 ORF8 show less luminescence in infected cells than VLPs produced in the absence of
183 ORF8 (**Fig. 3B**).

184

185 This can be interpreted as less cellular entry of the VLPs into the receiver cells or
186 a reduction in producing infectious particles. We, therefore, purified VLPs produced
187 either in the presence or absence of ORF8 on a 20% sucrose cushion and measured
188 the proteins contained in this fraction by western blot (**Fig. 3A**). By comparing the
189 amount of Spike and N proteins on the particles, we found that ORF8 expression leads
190 to a significant reduction of Spike protein loading and to a lesser extent of N protein
191 content in the secreted particles (**Fig. 3C-D).** This indicates that VLP production is
192 reduced when ORF8 is present in producer cells.

193 To examine further the possibility that virion entry is affected by ORF8, we
194 generated VLPs without ORF8 and incubated them with recombinant ORF8 before
195 infecting the receiver cells. We saw no difference in the receiver cells' luminescence or
196 viability (**Fig.S4A**), indicating that recombinant ORF8 does not interfere with VLP entry
197 into susceptible cells. We conclude that ORF8 interferes with VLP production in
198 producer cells but not entry into receiver cells.

199 We next asked whether ORF8 interacted with the structural proteins within VLP
200 producing cells. Co-immunoprecipitation experiments confirmed that ORF8 interacted
201 with the Spike but not with N in the VLP-producing cells (**Fig. 3E**). Due to antibody
202 issues, we could not determine whether ORF8 interacts with M and E during VLP
203 production. Notably, our analysis of the producer cells' lysates also showed that ORF8
204 expression decreased Spike expression in a dose-dependent manner in co-expressing
205 cells (**Fig. 3F**). This was also observed when we introduced 4-fold more of one of the
206 structural proteins (S, N, M, and E plasmids) together with steady amounts of ORF8 into
207 cells to exclude promoter competition or technical issues as an explanation (**Fig.S4 B-**

208 **D**). These findings confirm previous data that ORF8 reduces Spike protein expression
209 and show newly that this happens in VLP-producing cells independently of plasmid
210 amount or promoter competition.

211 Given that SARS-CoV-2 VLP production depends on specific Spike
212 concentrations, we can conclude that ORF8 reduces total VLP production (21). Notably,
213 we could not detect ORF8 in purified particles. This does not exclude the possibility that
214 ORF8 can bind Spike on virus particles. Together, these findings suggest that ORF8
215 specifically reduces Spike amounts in producer cells, thus hindering VLP production
216 and causing the release of fewer VLPs.

217 **The ORF8 signal peptide (aa 1–15) is sufficient to reduce VLP production.**

218 We tested whether the recent variants Delta or Omicron(BA.1) can escape
219 ORF8-mediated reduction in VLP production. Interestingly, we saw ORF8 efficiently
220 reduced VLP production in these variants **(Fig.S5).** In addition, we determined by site-
221 directed mutagenesis that none of the seven cysteine (C) residues that cause
222 intermolecular (C20) and intramolecular (C25 with C90, C37 with C102 and C61 with
223 C83) disulfide bonds within ORF8 are required for the Spike-suppressive activity of
224 ORF8 (**Fig.S6**).

225 To find the minimal region of ORF8 responsible for reducing VLP production, we
226 divided ORF8 into three distinct regions (aa 1–40, aa 41–80, and aa81–121), which we
227 cloned into an eGFP plasmid to produce eGFP-ORF8 fusion proteins. We also cloned
228 aa 1–7 and aa 1–26 of ORF8 into the eGFP plasmid, mimicking ORF8 from XBB.1.5
229 (G8Stop) and Alpha (Q27Stop) variants, respectively. We generated VLP in the

230 presence of these eGFP-ORF8 constructs. All constructs reduced VLPs production,
231 relative to the eGFP control plasmid, except for the aa 41-80 construct, which behaved
232 essentially like the eGFP control (**Fig. 4A**). Interestingly, having the first 26 aa was
233 enough to reduce VLP production nearly to the same extent as the full-length ORF8,
234 while having the first 7 aa reduced it by 50% (**Fig. 4A**). The fragments' effect on VLP
235 production mostly correlated with their ability to bind the Spike protein: we saw little to
236 no interaction between Spike and aa 1–7 or aa 41–80, but a strong interaction with aa
237 1–26 and aa 1–40 (**Fig.S7A**). This observation indicates that the first 26 aa of ORF8 are
238 sufficient to bind Spike and can cause a reduction in VLP production. Nevertheless,
239 Spike interaction with ORF8 is not necessary for reducing VLP production since aa 81–
240 121 strongly reduced VLP production even though it did not bind Spike. This last finding
241 underscores that at least two regions of ORF8 can inhibit VLP production: an N-terminal
242 portion that binds Spike, and a C-terminal portion that does not. Removal of 40 aa from
243 the N-terminal, middle, and C-terminal portions of ORF8 confirmed that only the N-
244 terminal portion is required to bind Spike (**Fig. 4B, S7B**). Since Alpha ORF8 has a stop
245 codon at position 27 in the N terminus, it still binds Spike, but the lack of the C-terminal
246 region reduces its additional suppressive effect on VLP production.

247 ORF8 has a 15 aa signal peptide at its N-terminus. Based on our data with the
248 truncated ORF8 of the XBB.1.5 and Alpha variants, we speculated that the signal
249 peptide might play a role in reducing VLP production. We therefore generated a
250 construct that only expresses the signal peptide of ORF8 and a construct that
251 expresses ORF8 without its signal peptide and tested their impact on VLP production.
252 The signal peptide alone significantly reduced VLP production (**Fig. 4C)**. The ORF8

253 devoid of signal peptide allowed more VLP production but did not fully rescue VLP
254 production, presumably because it retained the inhibitory C-terminal region of ORF8.
255 We also found that the ORF8 signal peptide reduced Spike levels and interacted with
256 Spike, while the ORF8 lacking the signal peptide did not (**Fig. 4D-E**). We performed a
257 triple alanine scan from aa 16 to 42 in ORF8, and found no changes in VLP production
258 or interaction with Spike (**Fig. S8A-C**). We conclude that the 15-aa ORF8 signal peptide
259 is sufficient to bind Spike and reduce VLP production.

260 **Restoration of ORF8 in XBB.1.5 reduces virus and VLP production.**

261 The recently emerged XBB.1.5, XBB.1.16, EG.1, and EG.5 lineages share the
262 G8Stop mutation in ORF8. To determine the relevance of the stop codon, we compared
263 XBB.1.5, and XBB.1.16 VLP production in the presence of full-length and truncated (aa
264 1-7) ORF8, compared to eGFP. We saw a significant reduction in VLP production with
265 full-length ORF8 but not with the truncated version, as expected (**Fig.5A**).

266 To further prove the importance of the stop codon for viral fitness, we restored
267 ORF8 expression in XBB.1.5 by converting the stop codon to Glycine (we refer to this
268 virus as IC-XBB.1.5+ORF8). In A549-ACE2 cells infected by this virus, we saw that
269 ORF8 colocalized with Spike and GM130, like we previously observed (**Fig.5B**). We
270 also observed fragmented Golgi morphology upon infection with IC-XBB.1.5+ORF8 but
271 not by XBB.1.5 (have truncated ORF8). When we infected Calu3 cells with both viruses,
272 we saw a significant reduction in particle production with IC-XBB.1.5+ORF8 virus at 72
273 hpi (**Fig.5C**). ORF8 expression in IC-XBB.1.5+ORF8 virus-infected cells was confirmed
274 (**Fig.5D**). These data indicate that the introduction of a stop codon at position eight as

275 seen in the XBB.1.5 variant is beneficial for infectious virus production. This supports
276 our model that ORF8 expression dampens viral particle production that deletions and
277 mutations affecting the signal peptide of ORF8 are evolutionary events that
278 counterbalance this suppression (**Fig.5E**).

279 **Discussion:**

280 Most studies so far have focused on the immunomodulatory and host-response
281 function of ORF8, less is known about the role ORF8 may play in the SARS-CoV-2
282 replication cycle. We have found that the signal peptide and the C terminal domain of
283 ORF8 can reduce SARS-CoV-2 virus production by hampering viral particle production.
284 Notably, we did not find any effects of ORF8 on entry and RNA replication steps. Our
285 work confirms findings from previous studies, including our own, that described an
286 interaction between Spike and ORF8, a reduction in Spike pseudovirus particle
287 productions, but also, importantly, extends our knowledge by showing ORF8 targeting
288 viral particle productions and causing Golgi fragmentations using live virus, replicon,
289 and VLP. While we contribute significant knowledge in VLP, replicon and virus-infected
290 cells, our study also opens several new areas of study..

291 Our model is that in SARS-CoV-2, which has intact ORF8 or produces signal
292 peptides of ORF8, viral particle production is dampened, possibly as a way to reduce
293 immunosurveillance of infected cells (14,16,30) or or as an unwanted effect of ORF8's
294 other functions benefitting viral replication (8,9,18) (**Fig 5E)**. In ORF8-deficient SARS-
295 CoV-2, viral particle production is not disrupted, leading to increased viral particle
296 formation (**Fig 5E)**. The effect on viral particle production happens through ORF8

297 binding Spike by its signal peptide. We also found that ORF8 expression in infected
298 cells can cause Golgi fragmentation.

299 In case of flavivirus infection, Dengue virus (DENV) NS1 protein can cause Golgi
300 stress as presented with Golgi dispersion and fragmentation (27). DENV NS1 also has
301 a 24 aa signal peptide sequence, forms dimer, and gets secreted as a soluble protein
302 (31,32). ORF8 signal peptide may be behaving in a similar way as NS1. Like NS1,
303 ORF8 can be secreted by conventional and unconventional secretory pathways (14,33).
304 Golgi morphology can change when Golgi stress response is activated to cope with
305 cells' capacity to mature, traffic, and secrete proteins using the Golgi network (34).
306 Secreted proteins cannot get secreted or delivered to the plasma membrane if Golgi
307 traffic is disrupted. Previously we saw reduced Spike co-localization in the trans-Golgi
308 network along with less Spike antigen on cells, when ORF8 and Spike are co-expressed
309 (16). It is plausible that ORF8 by itself or with other proteins, causes Golgi stress,
310 reducing Spike availability to be incorporated in viral particles, competing with virus for
311 its own secretion- hence reducing virus particles to form and exit out of infected cells.

312 At the same time, secreted ORF8 causes cytokine storms and activation of
313 inflammatory pathways (14,15). Patients vaccinated with inactivated SARS-CoV-2 have
314 anti-ORF8 antibodies in their serum- suggesting that the secreted ORF8 (probably in
315 the inactivated vaccine) can activate immune responses (30). Thus, the secretory
316 nature of ORF8 can bring more attention to virus-producing cells.

317

318 Many SARS-CoV-2 variants encode a truncated version of ORF8 or limit its
319 expression. The Singapore variant has almost a deleted ORF8, and it has been linked
320 to reduced severity (5). Similar isolates have been reported in other parts of the world,
321 such as Australia, Taiwan, and Bangladesh (35). Although these isolates did not
322 emerge as major variants, their presence shows the continuous evolution of SARS-
323 CoV-2. In recent lineages, ORF8 deletion or truncations are present in many sequences
324 (3,4) (**Fig. S1**). For sequences with full-length ORF8, such as BA.5 and XBC, it has
325 been observed that transcriptional regulatory sequences (TRS) contain a mutation that
326 is predicted to reduce ORF8 expression. Hisner et al. summarized and analyzed recent
327 variants with these ORF8 TRS mutations. They predicted that ORF8 ablation would
328 dominate in future lineages, while current lineages show reduced or removed ORF8
329 expression (4). The recent XBB.1.5, XBB.16, and EG.5 lineages express a truncated
330 ORF8, only the N-term 7 amino acids.

331 It is interesting to see that ORF8 is intact in its natural host. Comparing ORF8 of
332 Bat coronavirus (RaTG13) with SARS-CoV-2 ORF8 shows different interaction with
333 monocytes (36), suggesting a potential role for ORF8 in host adaptation. With these
334 truncations and deletions, it is plausible that SARS-CoV-2 evolution shapes minimal
335 ORF8 length for optimal viral replication in humans.

336

337

338

339 **Limitations of the study**

340 Due to antibody issues, we could not determine whether ORF8 might have some
341 roles in the other two structural proteins (M and E) during VLP production but we
342 successfully excluded interactions with N. While we show a role of ORF8 in viral particle
343 production, we are currently distinguishing between possible roles in viral assembly and
344 egress. We are keen to study the function of ORF8 in Golgi fragmentation and the role
345 of this function on viral assembly in future studies. Further investigation on this can lead
346 to an understanding of the biology of SARS-CoV-2 and the role of Golgi stress in viral
347 replication.

348

349

350

351

352

353

354

355

356

357

358 **Methods**

359 **Ethics**

360 We performed all research following all relevant ethical regulations. All work
361 conducted with replication-competent SARS-CoV-2 viruses was done in an approved
362 biosafety level 3 (BSL3) laboratory and experiments approved by the Institutional
363 Biosafety Committee of the University of California, San Francisco, and Gladstone
364 Institutes. The VLP and replicon work was done in an approved biosafety level 2 (BSL2)
365 laboratory.

366 **Virus**

367 SARS-CoV-2 USA-WA1/2020 (BEI NR-52281) and Singapore (EPI_ISL_414378)
368 clinical isolates were used for all live virus infection studies. All live virus experiments
369 were performed in a Biosafety Level 3 laboratory. The virus stocks were propagated in
370 Vero-E6 cells, and their sequence was verified by next-generation sequencing. Viral
371 stock titer was calculated using plaque-forming assays.

372 **Infectious clone and replicon generation**

373 Rep-WT, Rep-ORF8-stop, icXBB.1.5, and icXBB.1.5+ORF8 were generated
374 following pGLUE method in the pBAC SARS-CoV-2 construct as previously described
375 (22). Briefly, the SARS-CoV-2 genome was divided into 10 fragments, which were
376 cloned and later ligated via BsaI digestion and Golden Gate assembly protocol as
377 described by Taha et al (22,37). The ligated plasmid was confirmed via nanopore
378 sequencing (Primordium Labs). For XBB.1.5 infectious clone generation, BHK cells

379 were transfected with 3 µg of pBAC-SARS-COV-2 construct and1 µg of SARS-CoV-2 N
380 (Delta) plasmid with the X-treme Gene 9 (X9) DNA transfection reagent (Roche:
381 6365809001) was added 1:3 as DNA:X9. The supernatant was collected after 3 days
382 post-transfection and used to infect Vero ACE2 TMPRSS2 cells. The sup from infection
383 was passaged further to achieve high titer. All viruses generated in this study were
384 sequenced and verified by NGS. All infectious clone experiments were done in BSL3.
385 For replicon production, BHK cells were transfected with pBAC-SARS-COV-2 construct
386 (1), SARS-CoV-2 Spike (0.5), SARS-CoV-2 N (0.5), and ORF8(4) plasmid with
387 indicated molar ratio with Xtreme gene 9. In experiments where eGFP replaced ORF8,
388 eGFP amount was used half of ORF8 amount (ORF8 expression was lower than
389 eGFP), and supplemented with vector plasmid. The medium was replaced 12-16 hours
390 later and added fresh culture media. Medium-containing replicon was collected 48 and
391 72 hours later post-transfection. For infection, 100µl of replicon was used to infect Vero-
392 ACE2-TMPRSS2 cells. The cells were plated in 3X10^4 cells/well in 96 well plate the
393 day before infection. The day after infection, medium was replaced and 72 hours post-
394 infection 50µl of sup was used for nano-luciferase assay (Promega, N1120) according
395 to manufacturer protocol. Luminescence was measured using a TECAN plate reader
396 (Spark).with 30s shaking, auto attenuation, and 1000 ms integration. At least 3
397 independent experiments and infection were done in three technical replicates.

398 **Cell lines**

399 HEK293T, BHK-21, Calu3 and Vero-E6 were obtained from ATCC were cultured
400 in DMEM (Corning) supplemented with 10% fetal bovine serum (FBS) (GeminiBio), 1%
401 glutamine (Corning), and 1% penicillin-streptomycin (Corning) at 37°C, 5% CO2. Calu3

402 cells were cultured in Advanced (Gibco) supplemented with 2.5% FBS, 1% GlutaMax,
403 and 1% penicillin-streptomycin at 37°C, 5% CO2. A549 cells stably expressing ACE2
404 (A549-ACE2) were generated by transducing with ACE2-encoding (generated using
405 Addgene plasmid no. 154981, a gift from Sonja Best, Rocky Mountain Labs, Hamilton,
406 MT, USA) lentiviruses and selection with blasticidin (10 µg/mL) for 10 days. ACE2
407 expression was verified by Western blot. A549-ACE2 cells were cultured in DMEM
408 supplemented with 10% FBS, blasticidin (20 µg/ml) (Sigma), and maintained at 37°C
409 with 5% CO2. The HEK-293T ACE2-TMPRSS2 cell line was generated using sequential
410 transduction as described in (29). Vero stably coexpressing human ACE2 and
411 TMPRSS2 cells (gifted from A. Creanga and B. Graham, NIH, Bethesda, MD) were
412 cultured at 37 °C and 5% CO2 in DMEM (Gibco) supplemented with 10% fetal calf
413 serum, 100 ug/mL penicillin and streptomycin (Gibco), and 10 µg/mL of puromycin
414 (Gibco).

415 **Plaque forming assay**

416 Cell supernatants were analyzed for viral production using plaque-forming
417 assays. Vero ACE2 TMPRSS2 cells were used for the assay and plated 24 hr before
418 infection. Then the supernatants from producer cell cultures were serially diluted in
419 DMEM (Corning) and added on to the cells. After a 1 hr absorption period, 2.5% Avicel
420 (Dupont, RC-591) was overlaid. The overlay was removed 72 hours later, fixed in 10%
421 formalin for 1 hour, and stained with crystal violet for 10 minutes to visualize plaque
422 formation. All plaque assays were done in two technical duplicates from 3 independent
423 experiments.

424 **Plasmids**

425 The plasmids expressing SARS-CoV-2 ORF8 (ORF8-WT) were generous gifts
426 from Dr. Nevan Krogan (UCSF, The Gladstone Institutes). An ORF8-WT plasmid was
427 used as a source for generating all the mutated plasmids. Most of the ORF8 mutants
428 were generated by designing primers with the desired mutations, generating PCR
429 fragments with these primers and ligating them. The rest of them were generated with
430 custom gene fragments (gblock(IDT)). All these mutation-containing fragments, PCR
431 product or gblock, were ligated using NEBuilder HiFi DNA Assembly Master Mix
432 (E2621L). The ligated product was transformed to Mach1-competent cells. The
433 plasmids expressing SARS-CoV-2 Spike(S), Nucleocapsid (N), Membrane (M), and
434 Envelop (E) for VLP production were generous gifts from Prof. Jennifer A. Doudna (The
435 Gladstone Institutes). All plasmids used in this study are listed in Table 1. All plasmids
436 and corresponding sequence information are available upon request.

437 **VLP production, purification, and confirmation**

438 VLPs were produced by transfecting plasmids for all the structural proteins (S, N,
439 M-IRES-E(MiE)) and ORF8 or EGFP, along with a plasmid expressing firefly luciferase
440 with the SARS-CoV-2 RNA packaging signal(T-20), into HEK 293T cells, with a slight
441 modification to a previously described protocol (21). The HEK293T cells were seeded in
442 a 6-well with 0.5X10^6 cells/well. For transfection, S:N:MiE:T-20: ORF8/eGFP plasmids
443 with 0.125:0.67:0.33:1:0.4 DNA mass ratios for a total of 2.525 µg of DNA were diluted
444 in 150 µL OptiMEM. The X-treme Gene 9 (X9) DNA transfection reagent (Roche:
445 6365809001) was added 1:3 as DNA:X9 added to the plasmid dilution and mixed

446 properly. This mixture was incubated for 15 minutes at room temperature and then
447 added to cells. The culture media was replaced the next day. The culture media
448 containing VLP was collected 48 hours post-transfection, spun at 1000 rpm for 5
449 minutes, filtered through a 0.45 μm filter, and used immediately for infection or stored at
450 -80°C for later infection. This filtered supernatant is considered as VLP. For the
451 experiment, where different ORF8 plasmid amounts were used, a vector plasmid was
452 added to ensure the total ORF8+vector plasmid amount was 0.4μg. For infection, the
453 HEK293T-ACE2-TMPRSS2 cells (50K cells/condition) were mixed with 100 μl of VLP
454 and plated immediately in 96-Chimney opaque flat-bottom plates (Grenier). After 24
455 hours of incubation at 37°C, the cells were lysed with 30 μl/well of passive lysis buffer
456 (E1941) for 15 minutes. After that, 50 μl of luciferase assay buffer (Promega, E1501)
457 was added and luminescence was read using the TECAN plate reader (Infinite® 200
458 PRO) with auto attenuation, and 1000 ms integration.

459 To purify the VLPs, the transfection was done in 10 cm2 plates with the same
460 plasmid ratio with total 24.125ug of plasmid and 72.4ul of PEI was used as transfection
461 reagent. The filtered supernatant of producer cells (collected 48 hr after transfection)
462 was combined with 0.5–1 ml of a control lentivirus, placed in an ultracentrifuge tube and
463 a 20% sucrose solution (1/10 of total volume) was carefully added to the bottom of the
464 tube. PBS was added to adjust volume and balance, and the tubes were spun in an
465 SW32Ti at 24,000 rpm for 2 hours. The supernatant was decanted and the pellet dried
466 for 10 mins. The pellet was then resuspended in 90 ul RIPA Buffer (25 mM Tris-HCl pH
467 7.6, 150 mM NaCl, 1% NP-40, 1% sodium deoxycholate, 0.1% SDS) and analyzed by
468 western blot. The lentivirus served as a control for concentration. The control lentivirus

469 was produced with a 1:1:0.34 DNA ratio with plasmids pLVX-EF1α-IRES-Puro: psPAX2:
470 pMD2.6.

471 **Western blot analysis**

472 Cells were collected by spinning at 1000 rpm for 5 minutes, followed by a 1x PBS
473 wash. Cells were lysed in Flag lysis buffer (25 mM Tris-HCl pH 7.4, 150 mM NaCl, 1
474 mM EDTA, 1% NP-40, supplemented with Halt protease inhibitor cocktail). For infected
475 cells or purified VLP, RIPA buffer was used to obtain whole-cell lysates. The protein
476 concentration in the cell lysates was determined using a DC™ protein assay kit
477 (BioRad, 5000111). The same amounts of proteins were run on 4-20% Mini-
478 PROTEAN® TGX™ Precast Protein Gels (BioRad, Cat:4561096) or homemade 6-15%
479 SDS-PAGE gels and transferred to a nitrocellulose membrane (Biorad). The membrane
480 was blocked in 10% non-fat dry milk in TBS-T and stained with primary antibody
481 overnight at 4°C or 2-3 hours at room temperature. Blots were rinsed with TBS-T three
482 times for 5 minutes each and stained with secondary HRP antibody (Bethyl A90-516P
483 (mouse), A120-201P (rabbit) 1:5000). After that three washes were done with TBS-T.
484 The blot was incubated with a chemiluminescence kit (Roche 12015200001, Thermo
485 Scientific™ 34096) and images were captured using ChemiDoc™ Imaging System
486 (Biorad 12003153). Densitometry was done using ImageJ software. All the antibodies
487 used in this study are listed in Table 2.

488 **Immunoprecipitation**

489 Transfected HEK293T cells were collected at the 48 hr timepoint and lysed in IP
490 buffer (50 mM Tris-HCl, 150 mM NaCl, 1 mM EDTA, 1% NP40, supplemented with Halt

491 protease inhibitor cocktail). For pulldown, 0.5-1 mg of lysate was incubated overnight
492 with 30 ul of Strep-Tactin Sepharose resin (IBA Life Science, 2-1201-002), rotating at
493 4°C. Bound protein was washed five times with IP buffer and eluted with Strep-Tactin
494 elution buffer (IBA Life Sciences, 2-1000-025). Eluted samples were analyzed by
495 western blot.

496 **Immunofluorescence microscopy**

497 A549-ACE2 cells were infected with MOI 0.5 and plated onto 22 mm^2 no. 1.5
498 coverslips. Cells were fixed in 4% paraformaldehyde, permeabilized with methanol on
499 ice for 10 min, and blocked in 3% bovine serum albumin. Cells were then
500 immunostained with the antibodies indicated in Table 2. The coverslips were mounted
501 onto glass slides using ProLong Gold Antifade Mountant (Invitrogen, P36934) and
502 analyzed by confocal microscopy (Olympus FV3000RS) using a Olympus UPLAN S-
503 APO 60× OIL OBJ,NA1.35,WD0.15MM objective. The resulting Z-stack was
504 reconstructed and rendered in 3D using Imaris software (Oxford Instruments).

505 **VLP entry assay with recombinant ORF8**

506 Flag-tagged ORF8 (conc. 1.7mg/ml) was produced by Chempartner (Batch:
507 CP20210318-MA, diluted in a buffer containing 50 mM Tris, 200mM NaCl, 1mM DTT,
508 pH 8.0). We tested 2 concentrations 1ug/ml and 10ug/ml. Three independent batches of
509 VLPs were produced without ORF8, and 100 ul of each batch was incubated with
510 recombinant ORF8 for 1.5 hr at 37°C. This was used to infect HEK293T-ACE2-
511 TMPRSS2 cells that had been plated the day before. 24 hr after infection, cell viability

512 and infection was meaused using Cell titre Glo assay (Promega, G7571), and
513 Luciferase assay system (Promega, E1501).

514 **Quantification and statistical analysis**

515 The number of experiments and replicates are indicated in individual figure
516 legends. Data were processed and visualized using GraphPad Prism. All quantified data
517 are represented as mean ± SD, as indicated, and quantification details are available in
518 figure legends. Western blot band intensities were quantified using ImageJ.

519 **Data availability**

520 All data supporting the present study's findings are available in the article,
521 extended data and supplementary figures, or from the corresponding authors on
522 request. Source data are provided with this paper.

523 **Acknowledgments**

524 M.O. received support from the National Institutes of Health (U19AI135990), the
525 James B. Pendleton Charitable Trust, the Roddenberry Foundation, P. and E. Taft, and
526 the Gladstone Institutes. M.O. is a Chan Zuckerberg Biohub – San Francisco
527 Investigator. M.O. also thanks Fast Grants and the Innovative Genomics Institute for
528 their support. J.A.D. acknowledges support from the National Institutes of Health
529 (R21AI59666) and from the Howard Hughes Medical Institute and the Gladstone
530 Institutes. I.P.C. was supported by NIH/NIAID (F31 AI164671-01). M.M.K. and M.O.
531 highly acknowledge senior scientific editor Françoise Chanut for her valuable input in

editing the manuscript. We thank Chia-Lin Tsou and Tan Yee Joo for helping with shipment logistics for the Singapore isolate (EPI_ISL_414378).

Author contributions

Conceptualization: M.M.K., M.O.; Methodology and Investigation, M.M.K., I.P.C, F.W.S, T.Y.T., T.T., R.K.S., A,M.S., A.C., M.M.M., U.S.G., J.H., I.J.K., J.B.; Writing, M.M.K., M.O.; Analysis, M.M.K., I.P.C., Visualization, M.M.K., Isolate acquisition: S.W.F., G.R.K, L.R., L.F.P.N., Supervision Funding Acquisition, N.J.K., J.A.D., E.V., M.O.

Disclosure statement

No potential conflict of interest was reported by the author(s).

550 **Figures**

551 **Figure 1:** SARS-CoV-2 ORF8 reduces virus production but not genome replication. **A.**
552 Top: Schematic diagram of WA1 (BEI NR-52281) and Singapore clinical isolate
553 (EPI_ISL_414378). The Singapore isolate has a 382 nt deletion, comprising the 3' end
554 of ORF7b and removing almost all of the ORF8. Bottom: PFU assay of WA1 and
555 Singapore isolate in HEK293T-ACE2-TMPRSS2 (HEK293T-A/T) cells. hpi: hours post-
556 infection. **B.** Top: Schematic diagram of SARS-CoV-2 Spike-deleted replicon system. In
557 Rep-WT, the whole SARS-CoV-2 genome except the Spike region was cloned into the
558 pBAC vector using a pGLUE method previously developed by our lab (22). Spike is
559 replaced with eGFP-nLuc, which is a reporter for genome replication in producer cells
560 and infection in infected cells. The nLuc(Nano Luciferase) has a secretion signal
561 peptide, which allows quantification of replication or infection from the supernatant. In
562 Rep-ORF8-Stop, a stop codon at the second amino acid (K2Stop) prevents ORF8
563 synthesis. Bottom: genome replication for Rep-WT and Rep-ORF8-Stop plasmids.
564 Luminescence of cell culture supernatant at different time points, normalized to Rep-WT
565 condition at 48h time point. BHK-21 cells were transfected with different replicon
566 plasmids in the presence of the Nucleocapsid (N) of SARS-CoV-2 Delta variant. **C.**
567 Workflow for replicon production and infection experiment. BHK-21 cells are transfected
568 with a replicon plasmid, plasmids expressing Spike and N from the SARS-CoV-2 Delta
569 variant, and a plasmid expressing Strep-tagged eGFP (control) or Strep-tagged ORF8.
570 Supernatants are collected at 72hr time points and used to infect Vero-ACE2-TMPRSS2
571 cells, later the supernatant of the infected cells was used for luminescence. Cell lysates
572 are collected to confirm protein expression by western blot**. D.** Luminescence of culture

573 media of replicon-infected Vero-ACE2-TMPRSS2 cells at 72 hpi. For each independent
574 experiment, luminescence was normalized to the eGFP control condition. For each
575 condition, three technical replicates were done for luminiscence measurements with
576 total 3 independent experiments were done. Data are represented as means plus SD.
577 The P values were calculated by One-way ANOVA test (**B**), Two-way ANOVA test and
578 two tailed paired t test (**D**). *, $P \leq 0.05$; **, $P \leq 0.01$; ***, $P \leq 0.001$. n = 3 independent
579 experiments.

580 **Figure 2:** SARS-CoV-2 ORF8 co-localizes with Spike in cis-Golgi (GM130) and induces
581 stress in Golgi (appears disrupted and fragmented). A549-ACE2 cells were infected with
582 WA1 (BEI NR-52281) and Singapore (EPI_ISL_414378) clinical isolates.
583 Immunostaining was done with antibodies against ORF8 (Green), Spike (Turquoise)
584 and the cis-Golgi marker GM130 (Red). DAPI (Blue) was used to stain nuclei. White
585 dotted square area was enhanced three times. White bar = 8 μm. n = 3 independent
586 experiments.

587 **Figure 3:** SARS-CoV-2 ORF8 expression reduces the production of virus-like particles.
588 **A.** Schematic representation of virus-like particle (VLP) production, confirmation, and
589 quantification. Plasmids encoding SARS-CoV-2 (B.1 lineage) structural proteins
590 (S(Spike), N (nucleocapsid protein), MiE (membrane and envelope, expressed from the
591 same plasmid), and the SARS-CoV-2 packaging signal with firefly luciferase reporter (T-
592 20) were transfected in HEK293T cells, along with either a plasmid encoding a Strep-
593 tagged eGFP (control), or three different doses of a plasmid encoding a Strep-tagged
594 ORF8. VLP-containing culture media was collected 48 hr after transfection. This VLP
595 was either used to infect HEK293T-ACE2-TMPRSS2 cells (HEK293T-A/T) or purified on

596 20% sucrose cushion for further analysis. For infection in HEK293T-A/T (VLP receiving
597 cells), luminescence was measured from the cell 24 hr later. Cell lysates were collected
598 from transfected HEK293T cells (VLP producer cells). Both cell lysates, and purified
599 VLP were ran on SDS-PAGE gel to assess protein expression by western blot. **B.**
600 Luminescence readout of HEK293T-A/T cells infected with VLPs produced in the
601 presence of increasing amounts ORF8, normalized to the eGFP control. For each
602 condition, three technical replicates were done for luminescence measurements with
603 total 3 independent experiments were done. **C.** Western blot analysis of proteins in the
604 concentrated VLP fractions. P24 was added to the VLPs prior to sucrose purification as
605 a control for concentration. **D.** Spike and N amounts in concentrated VLP particles as a
606 function of ORF8 plasmid amounts, normalized to the eGFP control condition. Protein
607 amounts were derived from densitometry analysis of western blots. **E.** Western blot
608 analysis of HEK293T cells lysates (Input) and co-immunoprecipitation by Strep pull
609 down (IP:Strep). For immunoprecipitation, the same amount of cell lysate across all
610 conditions was pulled down with streptactin sepharose resin. **F.** Quantification of Spike
611 in the HEK293T cells lysates as a function of ORF8 plasmid dose. Spike abundance
612 was measured by densitometry analysis of western blots and normalized to the eGFP
613 control condition. Data are represented as means plus SD. The P values were
614 calculated by One-way ANOVA test. *, $P \leq 0.05$; **, $P \leq 0.01$; ***, $P \leq 0.001$; ns, not
615 significant. n = 3 independent experiments

616 **Figure 4:** Expression of the N-terminal 15 aa signal peptide of ORF8 reduces SARS-
617 CoV-2 VLP production. **A -C.** Normalized luminescence of VLP-infected cells. VLPs
618 were produced in the presence of different fragments of ORF8. The ORF8 fragments

619 were expressed as fusions to eGFP. Luminescence is normalized to the eGFP control
620 condition in each experiments. For each condition, three technical replicates were done
621 for luminescence measurements with total 3 independent experiments were done. FL =
622 Full Length, SP = Signal peptide. **D.** Expression of Spike and N protein in VLP-
623 producing cells. Densitometry of western blos was used for protein quantification. **E**.
624 Representative western blot of VLP-producing cells. Immunoprecipitation was done
625 using Strep pulldown. Data are represented as means plus SD. The P values were
626 calculated by One-way ANOVA test. *, $P \leq 0.05$; **, $P \leq 0.01$; ***, $P \leq 0.001$; ns, not
627 significant. n = 3 independent experiments.

628 **Figure 5:** Truncated ORF8 from XBB.1 variants increases VLP production. **A.**
629 Normalized luminescence of cells infected with VLPs from various XBB variants. VLPs
630 were produced in the presence of different ORF8s. For each condition, three technical
631 replicates were done for luminescence measurements with total 3 independent
632 experiments were done. **B.** A549-ACE2 cells were infected with recombinant XBB. IC-
633 XBB.1.5 (contains naturally occurring ORF8-G8Stop mutation) and IC-XBB.1.5+ORF8
634 (ORF8 full-length expression was restored by restoring Glycine at amino acid 8 position
635 in ORF8). Immunostaining was done with antibodies against ORF8 (Green), Spike
636 (Turquoise) and the cis-Golgi marker GM130 (Red). DAPI (Blue) was used to stain
637 nuclei. White dotted square area was enhanced three times. White bar = 8 μm. **C.**
638 Plaque forming assay in Calu3 cells infected with the recombinant XBB.1.5 virus. **D.**
639 Representative western blot of cells infected with recombinant XBB.1.5 virus. **E.** A
640 model summarizing the role of ORF8 hampering SARS-CoV-2 viral particle production.
641 In the presence of ORF8, ORF8 interacts with Spike, reducing its expression. We also

642 observed Golgi fragmentation and dispersion in isolates that express ORF8. This led to
643 disrupted viral particle production, reducing viral particle production. The signal peptide
644 sequence alone is enough to interact with spikes and reduce spike expression and viral
645 particle production. Without ORF8, all the structural proteins are properly expressed and
646 particle production is not hampered. We also observed intact Golgi in infected cells by
647 ORF8 deleted or truncated isolates. Thus leads to increased or normal levels of viral
648 particle generation. Data are represented as means plus SD. The P values were
649 calculated by One-way **(A)** ANOVA test, and Two-way (**C**) ANOVA test. *, $P \leq 0.05$; **, P
650 ≤ 0.01; ***, $P \leq 0.001$. n = 3 independent experiments.

651

652

653

654

655

656

657

658

659

660

661 **Fig 1:**

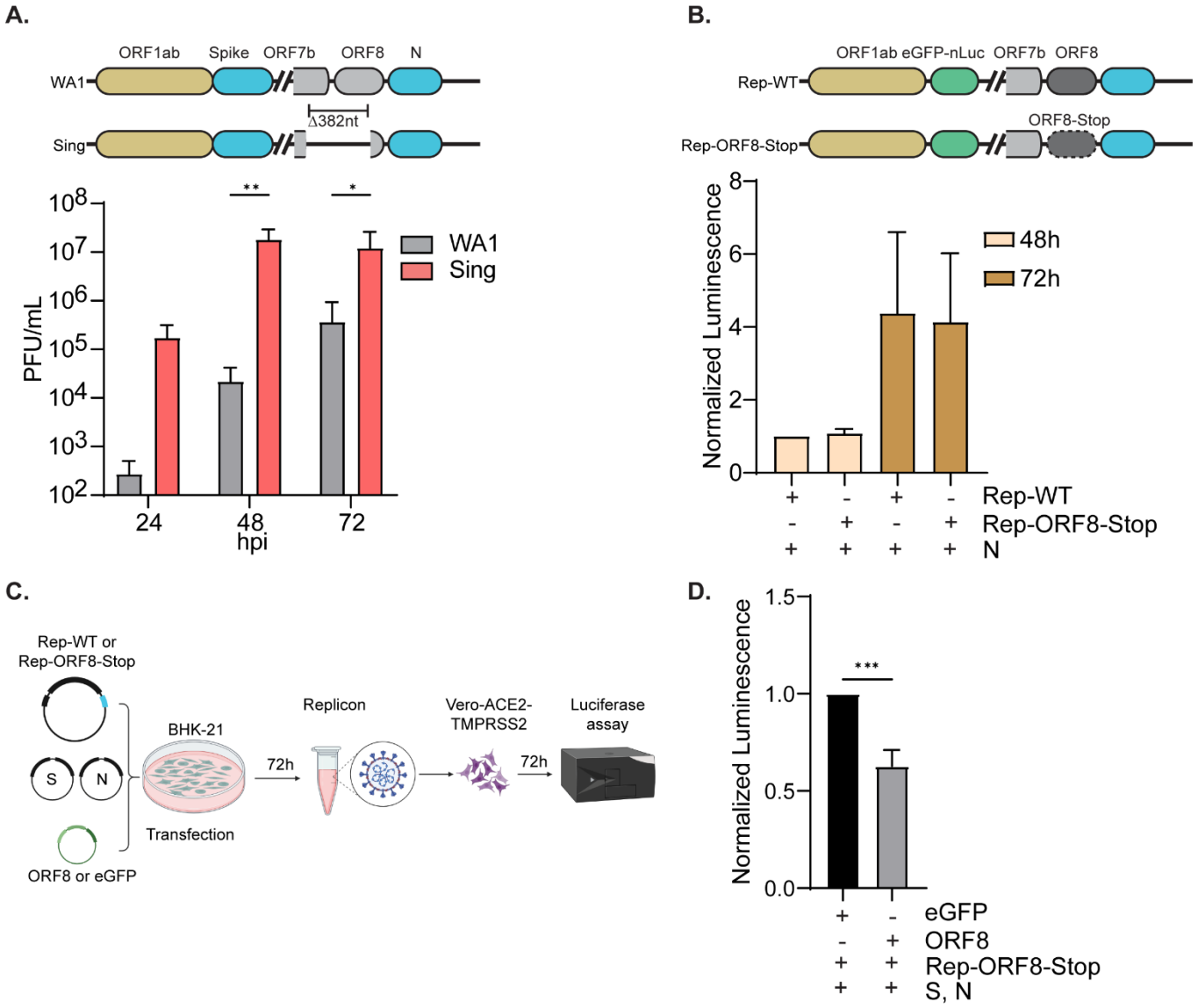

662

663

664

665

Fig 2:

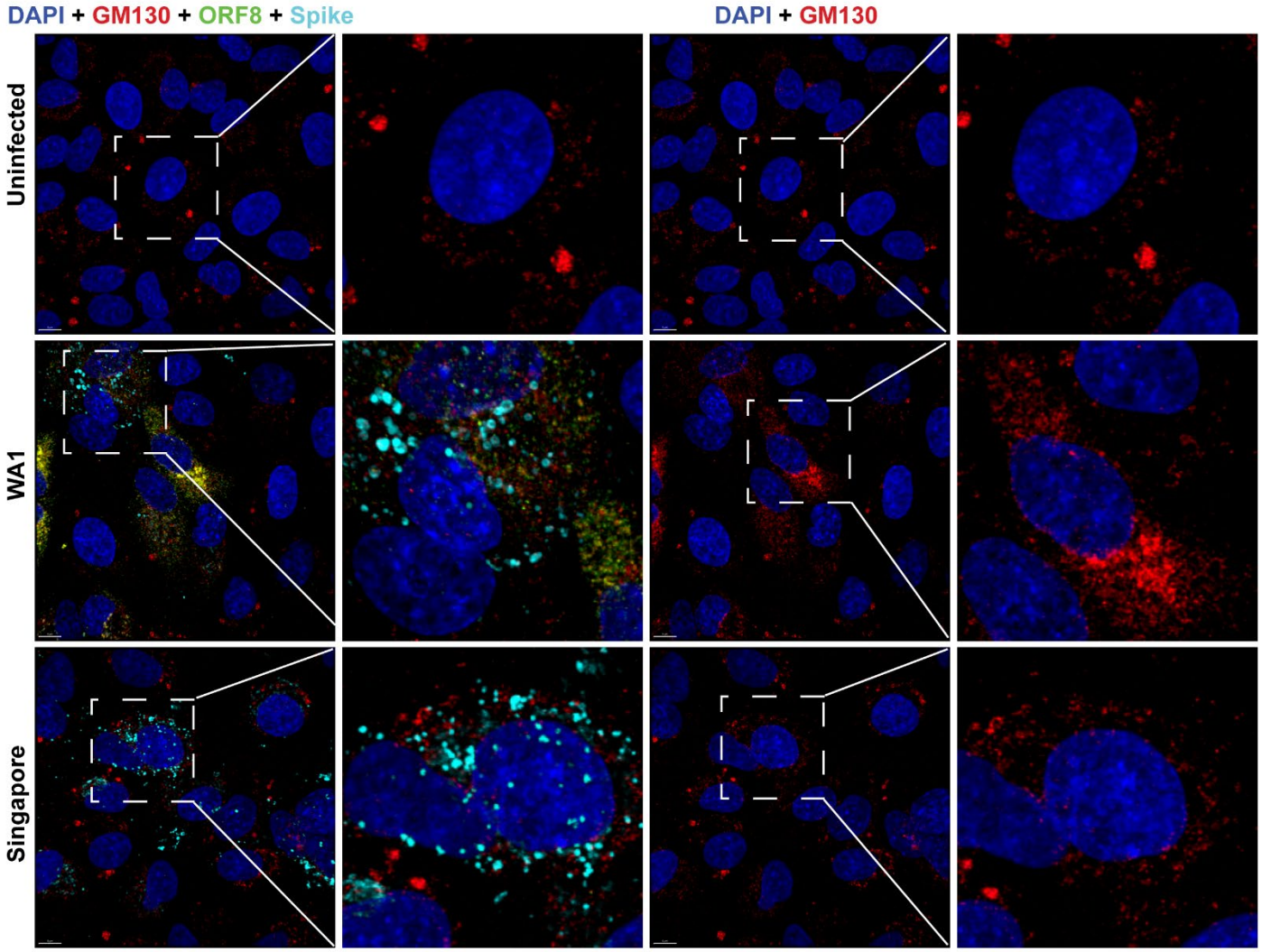

Fig 3:

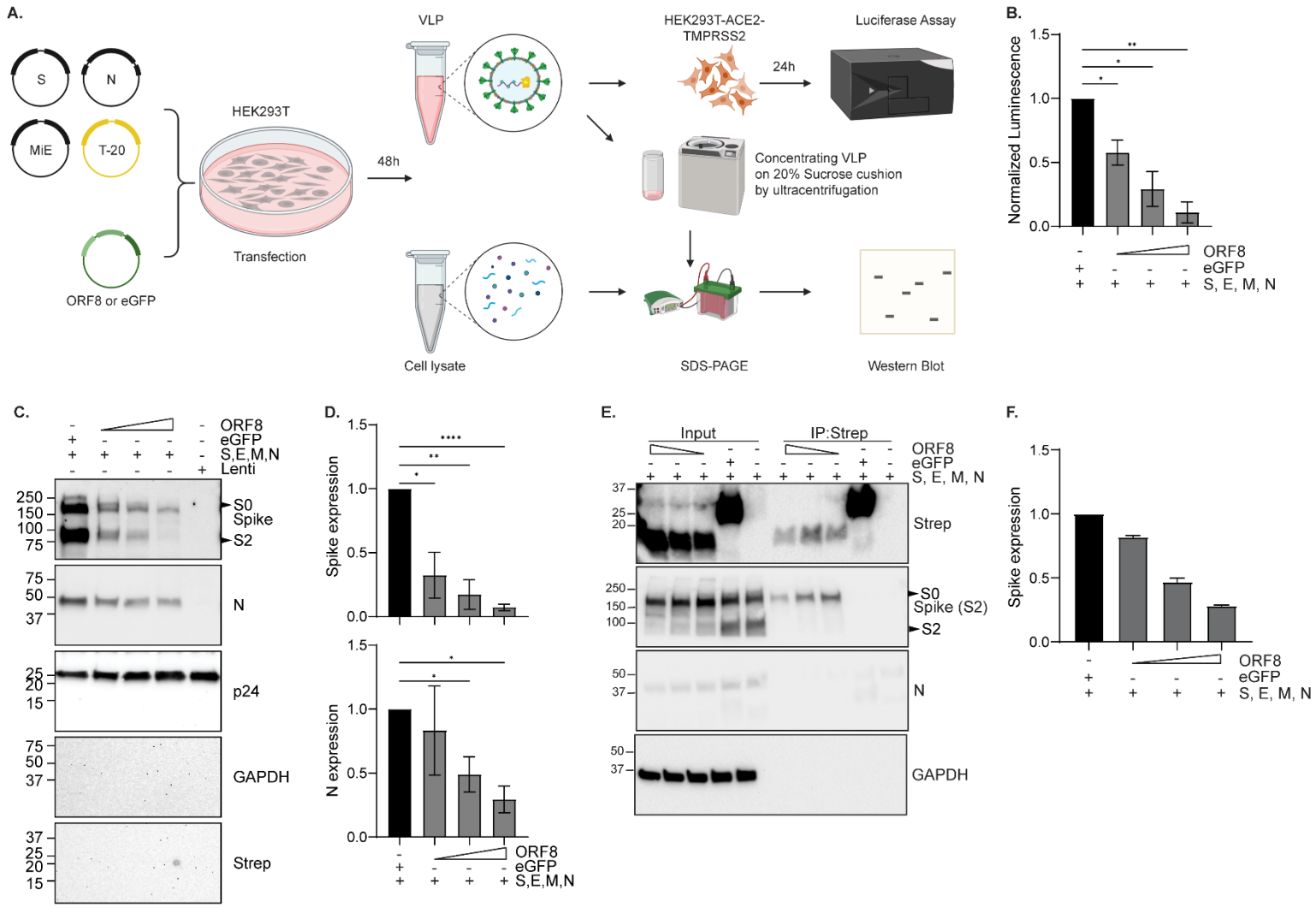
A.
S
N
MiE
T-20
ORF8 or eGFP
HEK293T
Transfection
48h
VLP
Cell lysate
HEK293T-ACE2-TMPRSS2
24h
Luciferase Assay
Concentrating VLP on 20% Sucrose cushion by ultracentrifugation
SDS-PAGE
Western Blot
B.
Normalized Luminescence
ORF8
eGFP
S, E, M, N
C.
ORF8
eGFP
S,E,M,N
Lenti
S0
Spike
S2
N
p24
GAPDH
Strep
D.
Spike expression
N expression
ORF8
eGFP
S,E,M,N
E.
Input
IP:Strep
ORF8
eGFP
S, E, M, N
Strep
S0
Spike (S2)
S2
N
GAPDH
F.
Spike expression
ORF8
eGFP
S, E, M, N

Fig 4:

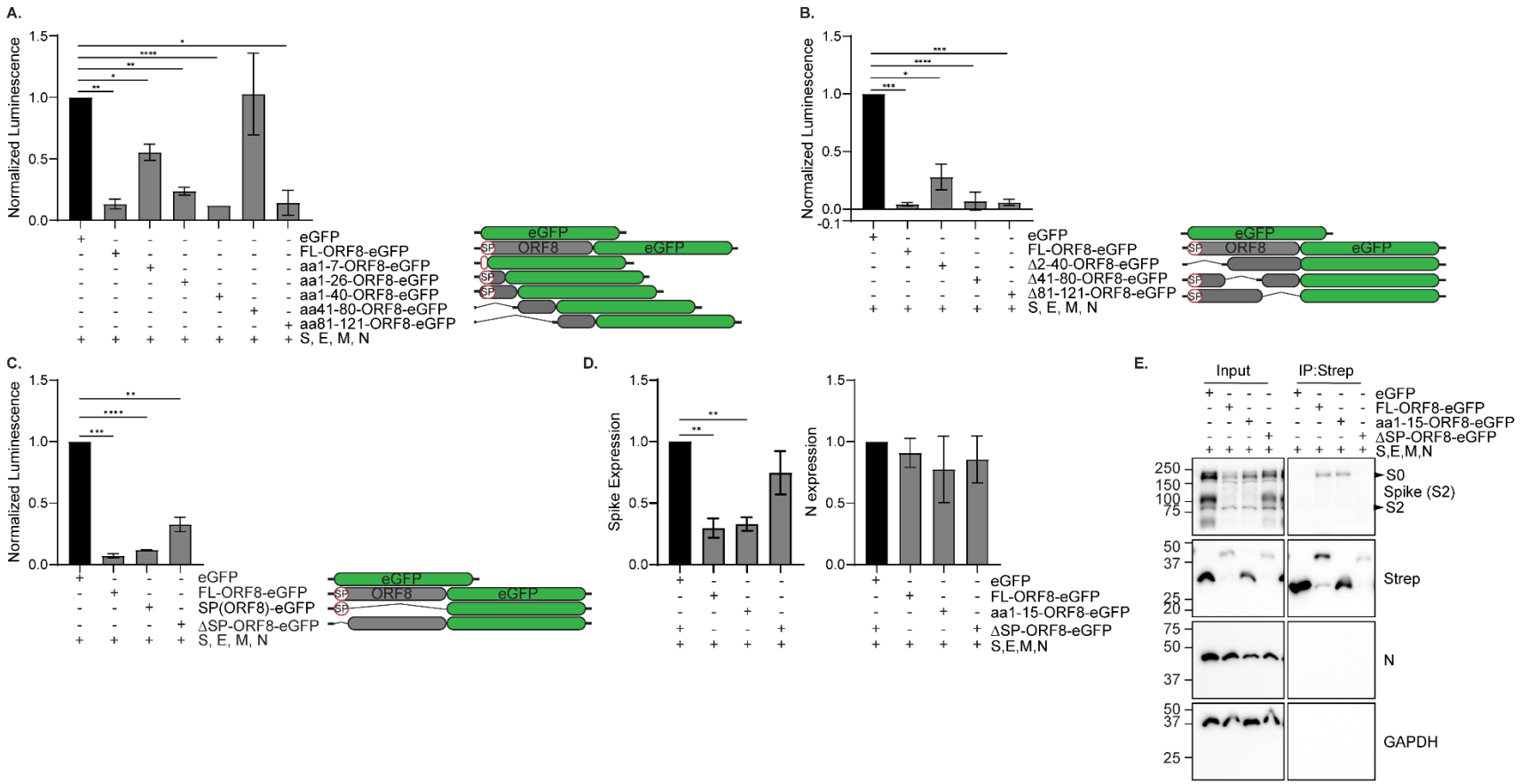
A.
Normalized Luminescence
eGFP
FL-ORF8-eGFP
aa1-7-ORF8-eGFP
aa1-26-ORF8-eGFP
aa1-40-ORF8-eGFP
aa41-80-ORF8-eGFP
aa81-121-ORF8-eGFP
S, E, M, N
B.
Normalized Luminescence
eGFP
FL-ORF8-eGFP
Δ2-40-ORF8-eGFP
Δ41-80-ORF8-eGFP
Δ81-121-ORF8-eGFP
S, E, M, N
C.
Normalized Luminescence
eGFP
FL-ORF8-eGFP
SP(ORF8)-eGFP
ΔSP-ORF8-eGFP
S, E, M, N
D.
Spike Expression
N expression
eGFP
FL-ORF8-eGFP
aa1-15-ORF8-eGFP
ΔSP-ORF8-eGFP
S,E,M,N
E.
Input
IP:Strep
eGFP
FL-ORF8-eGFP
aa1-15-ORF8-eGFP
ΔSP-ORF8-eGFP
S,E,M,N
S0
Spike (S2)
S2
Strep
N
GAPDH

672 **Fig 5:**

Figure 5: Restoration of ORF8 in XBB1.5 reduces virus production

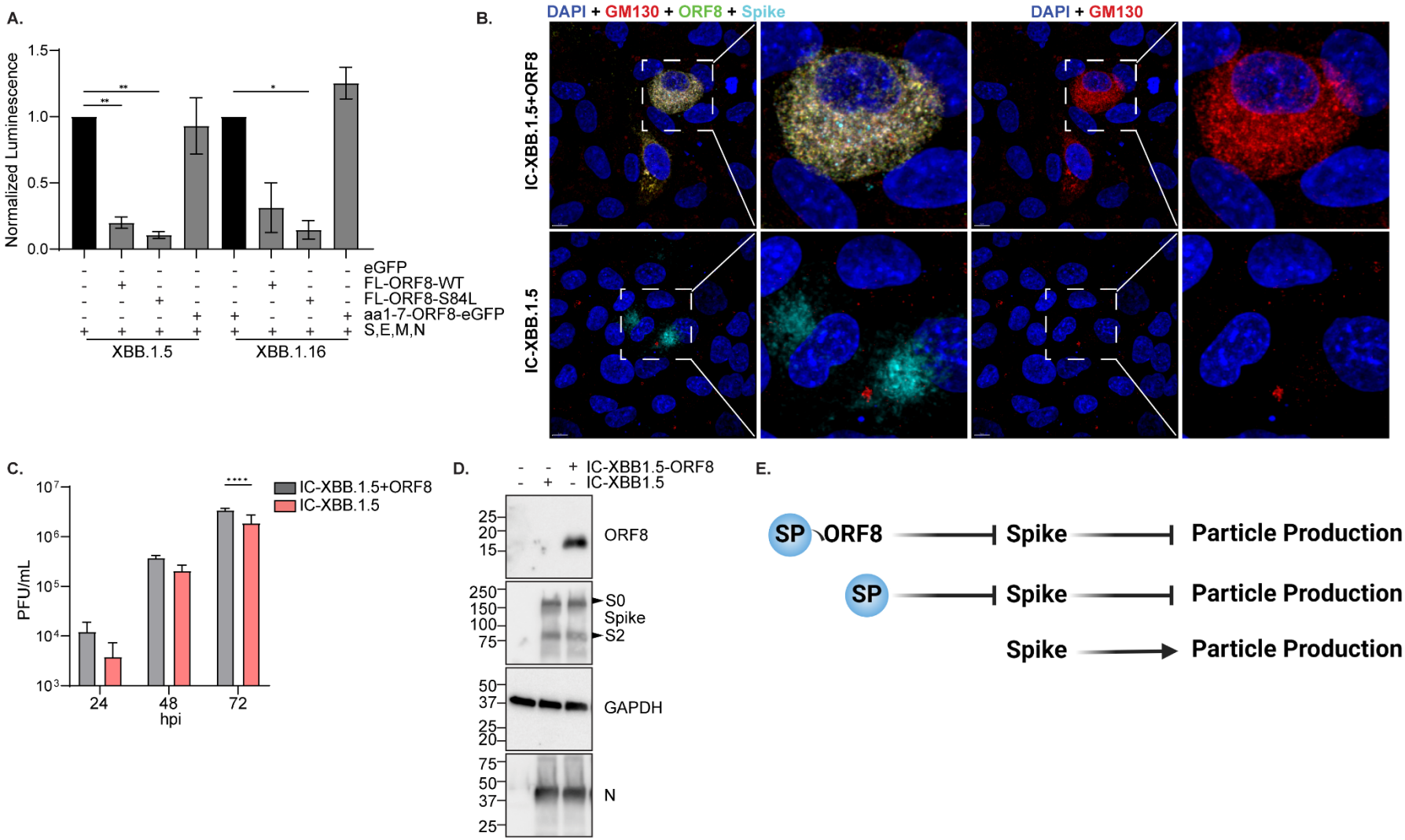

673

674 **Tables**

675 **Table 1:** List plasmids used in this study.

Plasmid name	content	Addgene No
pLVX-EF1a-IRES-Puro	Vector	N/A
eGFP-2xStrep	eGFP	141395
CoV2-Spike-D614G	B.1 Spike	177960
CoV2-Spike-Delta	Delta Spike	N/A
CoV2-Spike-Omicron	Omicron (BA.1) Spike	N/A
CoV2-Spike-XBB.1.5	XBB.1.5 Spike	N/A
CoV2-Spike-XBB.1.16	XBB.1.16 Spike	N/A
CoV2-N-B.1.1.7	B.1 N	177958
CoV2-N-Delta	Delta N	N/A
CoV2-N-Omicon	Omicron (BA.1) N	N/A
CoV2-N-XBB.1.5	XBB.1.5 N	N/A
CoV2-N-XBB.1.16	XBB.1.5 N (Same mutations)	N/A
CoV2-M-IRES-E	B.1 (M, and E)	177938
CoV2-M-IRES-E-Delta	Delta (M, and E)	N/A
CoV2-M-IRES-E-Omicon	Omicron (BA.1) (M, and E)	N/A
CoV2-M-IRES-E-XBB.1.5	XBB.1.5 (M, and E)	N/A
CoV2-M-IRES-E-XBB.1.16	XBB.1.5 (M, and E) (Same mutation)s	N/A
Luc-T20	Luciferase	177941
ORF8-FL-2Xstrep-eGFP	Full length ORF8 fused eGFP	N/A
ORF8-aa1-40-2Xstrep-eGFP	ORF8 aa2-40 fused eGFP	N/A

ORF8-aa41-80-2XStrep-eGFP	ORF8 aa41-80 fused eGFP	N/A
ORF8-aa41-121-2XStrep-eGFP	ORF8 aa41-121 fused eGFP	N/A
ORF8-Δ2-40-2Xstrep-eGFP	ORF8 except aa2-40 fused eGFP	N/A
ORF8-Δ41-80-2XStrep-eGFP	ORF8 except aa41-80 fused eGFP	N/A
ORF8-Δ41-121-2XStrep-eGFP	ORF8 except aa41-121 fused eGFP	N/A
ORF8-aa1-7-2Xstrep-eGFP	XBB.1.5 ORF8-fused eGFP	N/A
ORF8-aa1-26-2Xstrep-eGFP	Alpha ORF8-fused eGFP	N/A
ORF8-SP-2Xstrep-eGFP	ORF8 aa1-15 fused eGFP	N/A
ORF8-ΔSP-2Xstrep-eGFP	ORF8 except aa1-15 fused eGFP	N/A
ORF8-WT or ORF8-FL	Full length ORF8	141390
ORF8-C20A-2XStrep	FL-ORF8 with aa20 changed to Alanine	N/A
ORF8-C25A-2XStrep	FL-ORF8 with aa25 changed to Alanine	N/A
ORF8-C37A-2XStrep	FL-ORF8 with aa37 changed to Alanine	N/A
ORF8-C61A-2XStrep	FL-ORF8 with aa61 changed to Alanine	N/A
ORF8-C83A-2XStrep	FL-ORF8 with aa83 changed to Alanine	N/A
ORF8-C90A-2XStrep	FL-ORF8 with aa90 changed to Alanine	N/A
ORF8-C102A-2XStrep	FL-ORF8 with aa102 changed to Alanine	N/A
ORF8-NoCys-2XStrep	FL-ORF8 with all cysteine changed to Alanine	N/A
ORF8-S84L-2XStrep	FL-ORF8 with aa84 changed to leucine	N/A
ORF8-AAA-16-18	FL-ORF8 with triple Alanine substitution at amino acids 16-18	N/A
ORF8-AAA-19-21	FL-ORF8 with triple Alanine substitution at amino acids-AAA-19-21	N/A
ORF8-AAA-22-24	FL-ORF8 with triple Alanine substitution at amino acids-AAA-22-24	N/A
ORF8-AAA-25-27	FL-ORF8 with triple Alanine substitution at amino acids-AAA-25-27	N/A

ORF8-AAA-28-30	FL-ORF8 with triple Alanine substitution at amino acids-AAA-28-30	N/A
ORF8-AAA-31-33	FL-ORF8 with triple Alanine substitution at amino acids-AAA-31-33	N/A
ORF8-AAA-34-36	FL-ORF8 with triple Alanine substitution at amino acids-AAA-34-36	N/A
ORF8-AAA-37-39	FL-ORF8 with triple Alanine substitution at amino acids-AAA-37-39	N/A
ORF8-AAA-40-42	FL-ORF8 with triple Alanine substitution at amino acids-AAA-40-42	N/A
Rep-ORF8-WT	Spike deleted (replaced with eGFP-nLuc) Replicon (pBAC) plasmid of WA1 expressing ORF8	N/A
Rep-ORF8-Stop	Spike deleted (replaced with eGFP-nLuc) Replicon (pBAC) plasmid of WA1 with ORF8 having stop codon at 2nd amino acid	N/A
IC-XBB.1.5	Infectious clone (pBAC) plasmid of XBB.1.5 expressing trancated ORF8 (G8Stop)	N/A
IC-XBB.1.5+ORF8	Infectious clone(pBAC) plasmid of XBB.1.5 expressing full length ORF8	N/A

676

677 **Table 2:** List antibodies used in this study.

Antibody	**Manufacturer**	**Cat: No**
SARS-CoV2 Spike(S2)	Abcam	ab272504
SARS-CoV-2 Spike S1 Alexa 647	R&Dsystems	FAB105403R
SARS-CoV2 Spike Alexa 594	Novus Biologicals	NBP2-90980AF594
SARS-CoV2 Nucleocapsid (N)	Abcam	ab273434
SARS-CoV2 Nucleocapsid (N)	Sino-biological	40143-MM05
SARS-CoV2 ORF8	Abcam	ab283914
Anti-HIV-1 P24	Sigma Aldrich	SAB3500946
Strep Tag II	Qiagen	1023944
Flag	Sigma Aldrich	F3165
hACE2	Proteintech	28868-1-AP
hTMPRSS2	Abcam	ab109131
GAPDH	Cell Signaling	5174S
GAPDH	Santa Cruz	sc-365062
GM130- Alexa Fluor™ 555	ThermoFisher Scientific	PA1-077-A555
Hoescht 33342	Invitrogen	H3570
Mouse IgG-AlexaFluor549	Invitrogen	A11005
Rabbit IgG-AlexaFluor488	Invitrogen	A11008
Rabbit IgG-HRP	Bethyl	A120-201P
Mouse IgG-HRP	Bethyl	A90-516P

678 **References**

679 1. Chan JFW, Kok KH, Zhu Z, Chu H, To KKW, Yuan S, et al. Genomic characterization
680 of the 2019 novel human-pathogenic coronavirus isolated from a patient with atypical
681 pneumonia after visiting Wuhan. Emerg Microbes Infect. 2020 Jan 28;9(1):221–36.

682 2. Alkhansa A, Lakkis G, El Zein L. Mutational analysis of SARS-CoV-2 ORF8 during six
683 months of COVID-19 pandemic. Gene Rep. 2021 Jun 1;23:101024.

684 3. Zinzula L. Lost in deletion: The enigmatic ORF8 protein of SARS-CoV-2. Biochem
685 Biophys Res Commun. 2021 Jan 29;538:116–24.

686 4. Ryan Hisner, Federico Gueli, Thomas P. Peacock. Virological. 2023 [cited 2023 Dec
687 5]. Repeated loss of ORF8 expression in circulating SARS-CoV-2 lineages - SARS-
688 CoV-2 coronavirus. Available from: https://virological.org/t/repeated-loss-of-orf8-
689 expression-in-circulating-sars-cov-2-lineages/931

690 5. Young BE, Fong SW, Chan YH, Mak TM, Ang LW, Anderson DE, et al. Effects of a
691 major deletion in the SARS-CoV-2 genome on the severity of infection and the
692 inflammatory response: an observational cohort study. The Lancet. 2020 Aug
693 29;396(10251):603–11.

694 6. Tang X, Wu C, Li X, Song Y, Yao X, Wu X, et al. On the origin and continuing
695 evolution of SARS-CoV-2. Natl Sci Rev. 2020 Jun;7(6):1012–23.

696 7. Pereira F. SARS-CoV-2 variants combining spike mutations and the absence of
697 ORF8 may be more transmissible and require close monitoring. Biochem Biophys
698 Res Commun. 2021 Apr;550:8–14.

699 8. Zhang Y, Chen Y, Li Y, Huang F, Luo B, Yuan Y, et al. The ORF8 protein of SARS-
700 CoV-2 mediates immune evasion through down-regulating MHC-I. Proc Natl Acad
701 Sci. 2021 Jun 8;118(23):e2024202118.

702 9. Li JY, Liao CH, Wang Q, Tan YJ, Luo R, Qiu Y, et al. The ORF6, ORF8 and
703 nucleocapsid proteins of SARS-CoV-2 inhibit type I interferon signaling pathway.
704 Virus Res. 2020 Sep;286:198074.

705 10. Wang X, Lam JY, Wong WM, Yuen CK, Cai JP, Au SWN, et al. Accurate Diagnosis
706 of COVID-19 by a Novel Immunogenic Secreted SARS-CoV-2 orf8 Protein. mBio.
707 2020 Oct 20;11(5):e02431-20.

708 11. Lin X, Fu B, Yin S, Li Z, Liu H, Zhang H, et al. ORF8 contributes to cytokine storm
709 during SARS-CoV-2 infection by activating IL-17 pathway. iScience. 2021
710 Apr;24(4):102293.

711 12. Ponde NO, Shoger KE, Khatun MS, Sarkar MK, Dey I, Taylor TC, et al. SARS-CoV-
712 2 ORF8 Mediates Signals in Macrophages and Monocytes through MyD88
713 Independently of the IL-17 Receptor. J Immunol. 2023 Jun 2;211(2):252–60.

714 13. Wu X, Xia T, Shin WJ, Yu KM, Jung W, Herrmann A, et al. Viral Mimicry of
715 Interleukin-17A by SARS-CoV-2 ORF8. Damania B, editor. mBio. 2022 Apr
716 26;13(2):e00402-22.

717 14. Lin X, Fu B, Xiong Y, Xing N, Xue W, Guo D, et al. Unconventional secretion of
718 unglycosylated ORF8 is critical for the cytokine storm during SARS-CoV-2 infection.
719 Perlman S, editor. PLOS Pathog. 2023 Jan 23;19(1):e1011128.

720 15. Wu X, Manske MK, Ruan GJ, Witter TL, Nowakowski KE, Abeykoon JP, et al.
721 Secreted ORF8 induces monocytic pro-inflammatory cytokines through NLRP3
722 pathways in patients with severe COVID-19. iScience. 2023 Jun;26(6):106929.

723 16. Kim IJ, Lee Y ho, Khalid MM, Chen IP, Zhang Y, Ott M, et al. SARS-CoV-2 protein
724 ORF8 limits expression levels of Spike antigen and facilitates immune evasion of
725 infected host cells. J Biol Chem. 2023 Aug;299(8):104955.

726 17. Chou JM, Tsai JL, Hung JN, Chen IH, Chen ST, Tsai MH. The ORF8 Protein of
727 SARS-CoV-2 Modulates the Spike Protein and Its Implications in Viral Transmission.
728 Front Microbiol [Internet]. 2022 [cited 2023 Dec 5];13. Available from:
729 https://www.frontiersin.org/articles/10.3389/fmicb.2022.883597

730 18. Matsuoka K, Imahashi N, Ohno M, Ode H, Nakata Y, Kubota M, et al. SARS-CoV-2
731 accessory protein ORF8 is secreted extracellularly as a glycoprotein homodimer. J
732 Biol Chem. 2022 Mar;298(3):101724.

733 19. Flower TG, Buffalo CZ, Hooy RM, Allaire M, Ren X, Hurley JH. Structure of SARS-
734 CoV-2 ORF8, a rapidly evolving immune evasion protein. Proc Natl Acad Sci. 2021
735 Jan 12;118(2):e2021785118.

736 20. Gordon DE, Jang GM, Bouhaddou M, Xu J, Obernier K, White KM, et al. A SARS-
737 CoV-2 protein interaction map reveals targets for drug repurposing. Nature. 2020
738 Jul;583(7816):459–68.

739 21. Syed AM, Taha TY, Tabata T, Chen IP, Ciling A, Khalid MM, et al. Rapid
740 assessment of SARS-CoV-2–evolved variants using virus-like particles. Science.
741 2021 Dec 24;374(6575):1626–32.

742 22. Taha TY, Chen IP, Hayashi JM, Tabata T, Walcott K, Kimmerly GR, et al. Rapid
743 assembly of SARS-CoV-2 genomes reveals attenuation of the Omicron BA.1 variant
744 through NSP6. Nat Commun. 2023 Apr 21;14(1):2308.

745 23. Thi Nhu Thao T, Labroussaa F, Ebert N, V'kovski P, Stalder H, Portmann J, et al.
746 Rapid reconstruction of SARS-CoV-2 using a synthetic genomics platform. Nature.
747 2020 Jun;582(7813):561–5.

748 24. Zhang Y, Song W, Chen S, Yuan Z, Yi Z. A bacterial artificial chromosome (BAC)-
749 vectored noninfectious replicon of SARS-CoV-2. Antiviral Res. 2021 Jan
750 1;185:104974.

751 25. Kim BK, Choi WS, Jeong JH, Oh S, Park JH, Yun YS, et al. A Rapid Method for
752 Generating Infectious SARS-CoV-2 and Variants Using Mutagenesis and Circular
753 Polymerase Extension Cloning. Microbiol Spectr. 2023 Mar 6;11(2):e03385-22.

754 26. Scherer KM, Mascheroni L, Carnell GW, Wunderlich LCS, Makarchuk S, Brockhoff
755 M, et al. SARS-CoV-2 nucleocapsid protein adheres to replication organelles before
756 viral assembly at the Golgi/ERGIC and lysosome-mediated egress. Sci Adv. 2022
757 Jan 7;8(1):eabl4895.

758 27. Viettri M, Zambrano JL, Rosales R, Caraballo GI, Gutiérrez-Escolano AL, Ludert JE.
759 Flavivirus infections induce a Golgi stress response in vertebrate and mosquito cells.
760 Sci Rep. 2021 Dec 6;11(1):23489.

761 28. Zhang J, Kennedy A, Xing L, Bui S, Reid W, Joppich J, et al. SARS-CoV-2 triggers
762 Golgi fragmentation via down-regulation of GRASP55 to facilitate viral trafficking
763 [Internet]. Cell Biology; 2022 Mar [cited 2024 Jan 31]. Available from:
764 http://biorxiv.org/lookup/doi/10.1101/2022.03.04.483074

765 29. Syed AM, Ciling A, Taha TY, Chen IP, Khalid MM, Sreekumar B, et al. Omicron
766 mutations enhance infectivity and reduce antibody neutralization of SARS-CoV-2
767 virus-like particles. Proc Natl Acad Sci. 2022 Aug 2;119(31):e2200592119.

768 30. Cheng SMS, Lau JJ, Tsang LCH, Leung K, Lee CK, Hachim A, et al. Serological
769 assays for differentiating natural COVID-19 infection from vaccine induced immunity.
770 J Clin Virol. 2024 Feb;170:105621.

771 31. Falgout B, Chanock R, Lai CJ. Proper processing of dengue virus nonstructural
772 glycoprotein NS1 requires the N-terminal hydrophobic signal sequence and the
773 downstream nonstructural protein NS2a. J Virol. 1989 May;63(5):1852–60.

774 32. Flamand M, Megret F, Mathieu M, Lepault J, Rey FA, Deubel V. Dengue Virus Type
775 1 Nonstructural Glycoprotein NS1 Is Secreted from Mammalian Cells as a Soluble
776 Hexamer in a Glycosylation-Dependent Fashion. J Virol. 1999 Jul;73(7):6104–10.

777 33. Zhang S, He Y, Wu Z, Wang M, Jia R, Zhu D, et al. Secretory pathways and
778 multiple functions of nonstructural protein 1 in flavivirus infection. Front Immunol.
779 2023 Jul 13;14:1205002.

780 34. Kim WK, Choi W, Deshar B, Kang S, Kim J. Golgi Stress Response: New Insights
781 into the Pathogenesis and Therapeutic Targets of Human Diseases. Mol Cells. 2023
782 Apr;46(4):191–9.

783 35. Su YCF, Anderson DE, Young BE, Linster M, Zhu F, Jayakumar J, et al. Discovery
784 and Genomic Characterization of a 382-Nucleotide Deletion in ORF7b and ORF8
785 during the Early Evolution of SARS-CoV-2. mBio. 2020 Jul 21;11(4):e01610-20.

786 36. Chen X, Zhou Z, Huang C, Zhou Z, Kang S, Huang Z, et al. Crystal Structures of
787 Bat and Human Coronavirus ORF8 Protein Ig-Like Domain Provide Insights Into the
788 Diversity of Immune Responses. Front Immunol. 2021 Dec 17;12:807134.

789 37. Suryawanshi RK, Taha TY, McCavitt-Malvido M, Silva I, Khalid MM, Syed AM, et al.
790 Previous exposure to Spike-providing parental strains confers neutralizing immunity
791 to XBB lineage and other SARS-CoV-2 recombinants in the context of vaccination.
792 Emerg Microbes Infect. 2023 Dec 8;12(2):2270071.

793 38. Hadfield J, Megill C, Bell SM, Huddleston J, Potter B, Callender C, et al. Nextstrain:
794 real-time tracking of pathogen evolution. Bioinformatics. 2018 Dec 1;34(23):4121–3.

795 39. Emma B. Hodcroft. CoVariants: SARS-CoV-2 Mutations and Variants of Interest.
796 [cited 2024 Jan 2]. CoVariants: Variants. Available from:
797 https://covariants.org/variants

798